

Exciton Binding Energy in GaAs V-Shaped Quantum Wires

R. Rinaldi^(a) and R. Cingolani

Dipartimento di Scienza dei Materiali, Università di Lecce, I-73100 Lecce, Italy

M. Lepore, M. Ferrara, and I. M. Catalano

Dipartimento di Fisica, Università di Bari, I-70100 Bari, Italy

F. Rossi,^(b) L. Rota,^(c) and E. Molinari

Dipartimento di Fisica, Università di Modena, I-41100 Modena, Italy

P. Lugli

Dipartimento di Ingegneria Elettronica, Università Roma II, I-00173 Roma, Italy

U. Marti, D. Martin, F. Morier-Gemoud, P. Ruterana, and F. K. Reinhart

Ecole Polytechnique Fédérale de Lausanne, PHB Ecublens, CH-1015 Lausanne, Switzerland

(Received 20 May 1994)

We have determined the main parameters of the quasi-one-dimensional excitons confined in GaAs V-shaped quantum wires, namely exciton Bohr radius and binding energy, by two-photon absorption and magnetoluminescence experiments. The experimental results are in excellent agreement with our calculations, based on realistic wave functions for the actual wire geometry.

PACS numbers: 73.20.Dx, 78.66.Fd

Low dimensional semiconductor heterostructures are candidates of choice for basic quantum mechanical studies connected with the localization of the wave functions induced by the lateral potential [1]. In this Letter we determine the binding energy of the ground state exciton ($n_x = 1$) and of the first higher index exciton ($n_x = 2$) in V-shaped quantum wires, by means of two-photon absorption spectroscopy and magnetophotoluminescence. The obtained binding energies are related to the extension of the excitonic wave function, which is found to affect the strength of the characteristic diamagnetic shift of the exciton eigenstate in high magnetic field. A quantitative explanation of our results is obtained by calculating the electronic wave functions of the wire, by direct solution of the full two-dimensional (2D) Schrödinger equation for the real shape of the confining potential as deduced by transmission electron microscope (TEM) micrographs. The wave functions are then used to calculate the exciton binding energy according to a recently proposed model [2].

Our samples consist of large arrays (about 0.5 cm^2) of quantum wires grown by molecular-beam epitaxy (MBE) on GaAs substrates patterned by holographic lithography (257 nm line of an Ar^+ laser) and subsequent wet etching. The resulting V-shaped grooves were 250 nm wide and 120 nm deep. The wires originated from the bending of a GaAs quantum well (nominal thickness 3 nm) embedded in two $(\text{GaAs})_8/(\text{AlAs})_4$ superlattices, both grown in the grooves [3,4,5]. In the following, z is assumed to be the free wire direction, y is the growth axis of the sample, and x is the lateral-confinement direction. The nonlinear absorption has been studied by measuring the two-photon absorption-induced photoluminescence excitation

spectra (TPA-PLE) at 10 K for different polarization directions of the exciting laser beam (see Ref. [6] for experimental details). Magnetoluminescence experiments were performed by using the green line of an Ar^+ laser with the sample immersed in liquid He, at 3.5 K, in a superconducting cryostat (Oxford Spectromag 4000) providing magnetic fields up to 9.5 T. The spectral resolution was better than 0.8 \AA .

In Fig. 1(a) we show the photoluminescence (PL) spectrum of a 20 nm quantum-wire sample at 10 K. The experimental spectrum exhibits distinct emission bands from the $n_x = 1$ and $n_x = 2$ excitons. The vertical lines indicate the transition energies calculated according to the confinement energies quoted in Table I (see below). The power density in this measurement has been increased up to 4 W cm^{-2} in order to obtain the band filling of the second subbands [7]. The linear PL spectrum is compared to the TPA-PLE spectra in Fig. 1(b). Two-photon spectroscopy in quantum wires shows strongly anisotropic selection rules, depending on the relative orientation of the laser polarization vector ϵ , with respect to the quantization direction x [6,8,9]. In the $\epsilon \parallel x$ geometry, $1s$ excitons associated with $\Delta n_x = \pm 1, \pm 3$ transitions are allowed as final states of the nonlinear absorption process. On the contrary, $2p$ excitons associated with $\Delta n_x = 0$ transitions are expected in the $\epsilon \perp x$ configuration. The complementarity of these selection rules with the one-photon process allows one to directly measure the $2p$ - $1s$ splitting of the confined excitons and to observe otherwise forbidden transitions involving subbands with different quantum numbers.

The experimental $\epsilon \perp x$ spectrum of Fig. 1(b) exhibits two structures whose relative splitting reflects the energy

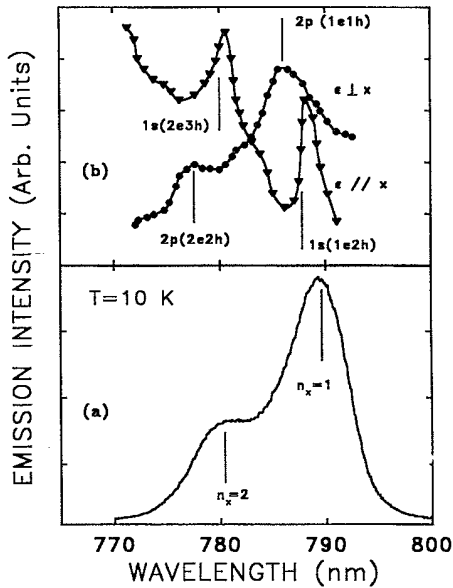


FIG. 1. (a) Linear photoluminescence spectrum measured at 10 K under continuous wave excitation (Ar^+ laser). (b) Two-photon absorption-induced photoluminescence excitation spectra (TPA-PLE) measured in the $\epsilon \perp x$ and $\epsilon \parallel x$ configurations (triangles and dots, respectively). $1s$ and $2p$ label the final exciton state associated with electron (e) and hole (h) subbands of quantum number n_x in the wire. The vertical lines indicate the transition energies calculated according to the confinement energies quoted in Table I.

separation between the two first $\Delta n_x = 0$ transitions observed in the linear spectrum. The peaks in the TPA curve are blueshifted with respect to the excitonic features of the linear PL curve, as expected for the $2p$ excited states. The blueshift amounts to about 7.5 ± 1 meV for the lowest energy transition ($1e-1h$) and to about 6 ± 1 meV for the higher index state ($2e-2h$ transition).

In the $\epsilon \parallel x$ configuration, the TPA-PLE spectrum shows two different structures. The relative splitting of the peaks is reasonably consistent with the energy positions of the $1s$ exciton states associated with $\Delta n_x = \pm 1$ transitions in the quantum wire, as expected for the present polarization geometry. The theoretical transition energies [vertical markers in Fig. 1(b)] were obtained by adding the confinement energies of the one-dimensional

TABLE I. Electron and hole lateral confinement energies (E_e and E_h , respectively) and exciton binding energies (E_b) for states of different quantum number n_x (theo = theoretical, MGL = magnetoluminescence, TPA = two-photon absorption). All values are quoted in meV.

	E_e^{theo}	E_h^{theo}	$E_b(\text{TPA})$	$E_b(\text{MGL})$	E_b^{theo}
$n_x = 1$	43.31	10.04	10 ± 1	12.5	11.7
$n_x = 2$	57.28	14.41	8 ± 1	9.7	8.9

(1D) conduction and valence subbands (Table I) to the $1s$ state of the $n_x = 1$ exciton.

From these data we can evaluate the exciton binding energy (E_b) of the $n_x = 1$ and $n_x = 2$ excitons in the investigated quantum wires. As demonstrated theoretically [10,11], the exciton binding energy of a perfectly 1D exciton scales like $E_b^p = -Ry/\nu^2$ (Balmer series), where ν is the principal quantum number, and Ry is the bulk Rydberg. Therefore, neglecting the $2p-2s$ angular momentum splitting, the $2p$ exciton is expected to have a binding energy equal to one-fourth of the ground state exciton binding energy. This gives for the $n_x = 1$ exciton $E_b = (E^{2p} - E^{1s})/0.75 = 10 \pm 1$ meV. Similarly, for the $n_x = 2$ exciton, we get $E_b = 8 \pm 1.5$ meV.

The above data indicate that the higher index excitons have more delocalized wave functions with respect to the $n_x = 1$ exciton. Though expected, this difference is more dramatic than in rectangular or cylindrical quantum wires. Indeed, in this case not only the lateral confining barriers reduce with increasing the energy of the subband but also the electron and hole wave functions become more delocalized due to the crescent shape of the quantum wires. This results in a $n_x = 1$ exciton are strongly localized at the bottom of the quantum wire. Conversely, the higher index states, formed by carrier wave functions of enlarged spatial extent, have a larger average correlation length for the relative motion of the electrons and hole, which causes the observed reduction of the binding energy of the $n_x = 2$ exciton.

The direct consequence of the increasing delocalization is the larger diamagnetic shift of the exciton in magnetic field. In Fig. 2 we display the energy shift of the $n_x = 1$ and $n_x = 2$ excitons recorded in backscattering (full dots) and edge (empty dots) configuration, as a function of the magnetic field (no $n_x = 2$ emission can be detected from the edge due to self-absorption). In the backscattering configuration ($B \parallel y$) the confined exciton experiences the lateral confinement along x , while in the edge configuration ($B \parallel x$) the exciton feels the quantum well confinement [12]. The observed diamagnetic shifts of the $n_x = 1$ band were fitted by means of the usual dependence [12]: $\Delta E = 4\pi^2 \hbar^4 \epsilon^2 / e^2 \mu^3 B^2$, where the exciton reduced mass μ is a fitting parameter, and $\epsilon = 12.6$ is the GaAs static dielectric constant. The different strength of the shift accounts for the anisotropy of the exciton wave function along the x and y directions. The best-fit values for the reduced masses are $\mu_x = 0.09m_0$ (in the $z-x$ plane), and $\mu_y = 0.153m_0$ (in the $y-z$ plane), giving the exciton Bohr radius $a_{0x} = 72 \text{ \AA}$, and $a_{0y} = 42 \text{ \AA}$. In order to evaluate the exciton binding energy, $E_b = e^4 \mu / 32\pi^2 \hbar^2 \epsilon^2$, we took $1/\mu = (1/\mu_x + 1/\mu_y + 1/\mu_z)/3$, where μ_z was estimated by scaling our data with those of Ref. [12]. The resulting reduced mass $\mu = 0.139m_0$ (to be compared with $\mu_0 = 0.055$ in the bulk) was multiplied by a factor of 0.769 to account for the difference between the cyclotron

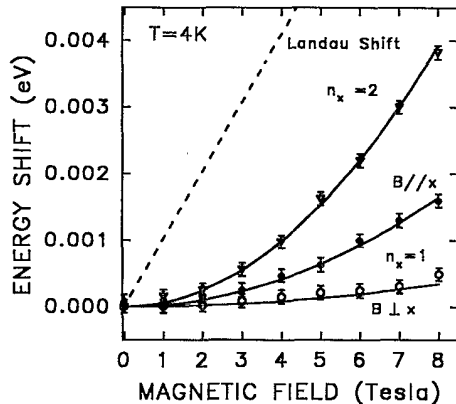


FIG. 2. Diamagnetic shift of the quasi-one-dimensional $n_x = 1$ (dots) and $n_x = 2$ (triangles) excitons of the quantum wires. The continuous curves represent the best-fit diamagnetic shift (see text), whereas the dashed line is the expected Landau shift for the GaAs. The full dots and empty dots represent the diamagnetic shifts measured with the magnetic field parallel and perpendicular to the carrier confinement direction ($B||x$ and $B||y$, respectively).

hole mass and the calculated nonparabolic hole mass, according to Ref. [13], yielding the value $\mu = 0.139m_0$ (to be compared with $\mu_0 = 0.055$ in the bulk). On the basis of these data, we find a binding energy of the ground state exciton $E_b = 12.5$ meV, in good agreement with the value estimated by the TPA-PLE measurements. Similarly, we have analyzed the larger diamagnetic shift of the $n_x = 2$ exciton displayed in Fig. 2 (triangles) [11]. In this case, the best-fit reduced mass in the x - y plane results $\mu_x = 0.067m_0$, giving a Bohr radius about 25% larger than that of the $n_x = 1$ exciton. The resulting binding energy was $E_b = 9.7$ meV.

To quantitatively account for the above experimental results, we have performed a theoretical investigation of both the electronic and excitonic properties of our wire structure. The system has been modeled in terms of the usual envelope-function approximation, and the carrier confinement has been described in terms of a z -independent 2D potential profile $V_{e/h}^c(x, y)$, as deduced from the quantum wire configuration observed by TEM micrographs. Within such a scheme, the three-dimensional electron (hole) envelope function can be factorized in terms of a plane wave along the free z direction and an envelope function $\psi_{e/h}(x, y)$, solution of the 2D Schrödinger equation with potential $V_{e/h}^c$. The latter has been solved numerically by direct diagonalization in terms of a plane-wave expansion [15]. Figure 3 shows the carrier distribution $|\psi(x, y)|^2$ corresponding to the first three electron subbands of the wire. As we can see, with increasing subband index, the wire wave functions become strongly delocalized and, in particular, this delocalization takes place along the x confinement direction. The result for the holes is very similar. The electron and hole energy levels obtained from our calculation (Table I) are in

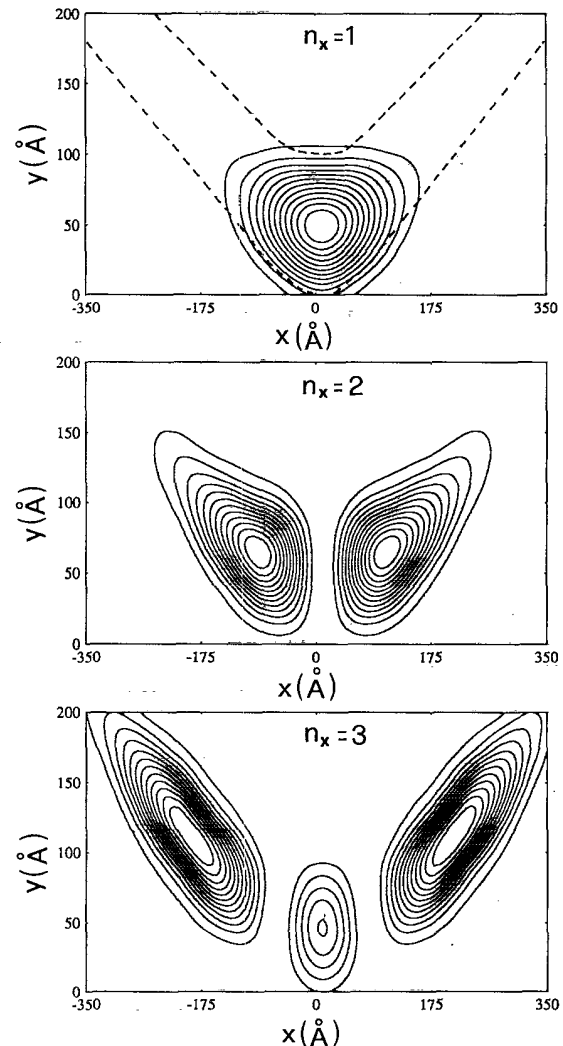


FIG. 3. Contour plot of the charge density probability $|\psi(x, y)|^2$ associated with the first three conduction subbands of the investigated quantum wires. The dashed lines represent the wire section in real space.

excellent overall agreement with the experimental transition energies of Fig. 1.

The wave functions of Fig. 3, together with the corresponding ones for holes, have been used to calculate the exciton binding energy of the investigated wires. Our analysis is based on the phenomenological fractional dimensional model, which was shown to reproduce quite accurately the results of variational approaches [2]. Following Ref. [2], we introduce an effective radial wave function $\chi_{e/h}(\rho)$ for electrons and holes, defined as the average over the angular coordinate θ of our wire wave function $\psi(\rho, \theta)$ [here ρ and θ denote a set of polar coordinates within the (x, y) plane]. We can then define an electron-hole correlation function

$$W(\rho) = 2\pi\rho \int_0^\infty |\chi_e(\rho_e)\chi_h(\rho_e \pm \rho)|^2 2\pi\rho_e d\rho_e, \quad (1)$$

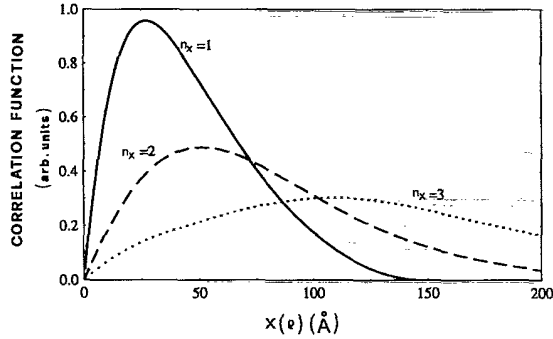


FIG. 4. Correlation function $W = W(\rho)$ of the first three electron and hole subbands in the investigated quantum wires.

which describes the probability of finding an electron-hole pair with relative distance ρ . Figure 4 shows the particular shape of the correlation function W for the first three electron and hole subbands. Again, we see an increase of the electron-hole delocalization with increasing n_x ; this is a direct consequence of the separate delocalization of both electrons and holes, as already pointed out in discussing Fig. 3. If we define $\bar{\rho}$ as a sort of average in-plane electron-hole distance, $\bar{\rho} = [\int_0^\infty \rho^2 W(\rho) d\rho]^{1/2}$, the effective exciton radius becomes $a_\perp = (1/a_0^2 + 1/\bar{\rho}^2)^{-1/2}$, where a_0 is the three-dimensional exciton Bohr radius. Following again Ref. [2], the desired exciton binding energy is $E_b^\nu = [\nu + (\alpha - 3)/2]^{-2}$ Ry, where ν denotes the principal quantum number, and $\alpha = 1 + 2(a_\perp/a_0)^{1/3}$.

Table I contains the values of E_b corresponding to the first wire subbands. The theoretical values of the binding energies compare very well with the data determined by TPA and magnetoluminescence spectroscopy. The binding energy of the one-dimensional ground level exciton (20 nm wire width) is enhanced by about 25%, with respect to the quantum well from which the wires originate. We want to stress that this simplified model does not take into account the strong in-plane anisotropy of our quantum wires. However, the excellent agreement between theoretical and experimental results indicates that the effective radial wave functions are the essential ingredients for the description of the exciton binding energies, provided that they are derived from realistic $\psi_{e/h}(\rho, \theta)$ wave functions.

In conclusion, we have studied excitons in V-shaped quantum wires both experimentally and theoretically. Two-photon absorption and magnetophotoluminescence spectroscopy reveal a decrease of the binding energy of the higher index one-dimensional excitons in the crescent-shape quantum wires. This is explained by the increasing delocalization of the electronic wave functions obtained by solving the full 2D Schrödinger equation for the

examined samples. Finally, the calculated exciton binding energies are found to be in good agreement with the measured values.

This work was partially supported by the European Community through the Esprit Project NANOPT.

^(a)On leave from Dipartimento di Fisica, Università di Bari I-70100 Bari, Italy.

^(b)Present address: Fachbereich Physik, Phillips Universität Marburg, Renthof 5, D-35032 Marburg, Germany.

^(c)Present address: Department of Physics, Clarendon Laboratory, Oxford OX1 3PU, England.

- [1] R. Cingolani and R. Rinaldi, *Rivista Nuovo Cimento* **16**, 1 (1993).
- [2] P. Christol, P. Lefebvre, and H. Mathieu, *J. Appl. Phys.* **74**, 5626 (1993).
- [3] M. Gailhanou, T. Baumbach, U. Marti, P.L. Silva, F.K. Reinhart, and M. Illegems, *Appl. Phys. Lett.* **62**, 1623 (1993).
- [4] E. Kapon, D.M. Hwang, and R. Bhat, *Phys. Rev. Lett.* **63**, 430 (1989); E. Kapon *et al.*, *Appl. Phys. Lett.* **60**, 477 (1992); M. Walther *et al.*, *Phys. Rev. B* **45**, 6333 (1992).
- [5] J. Christen, E. Kapon, E. Colas, D.M. Hwang, L.M. Schiavone, M. Grundmann, and D. Bimberg, *Surf. Sci.* **267**, 257 (1992); J. Christen *et al.*, *Phys. Status Solidi B* **173**, 307 (1992).
- [6] R. Cingolani, M. Lepore, R. Tommasi, I.M. Catalano, H. Lage, D. Heitmann, K. Ploog, A. Shimizu, H. Sakaki, and T. Ogawa, *Phys. Rev. Lett.* **69**, 1276 (1992).
- [7] R. Cingolani, *Phys. Scr.* **T49**, 470 (1993).
- [8] H.N. Spector, *Phys. Rev. B* **35**, 5876 (1987).
- [9] A. Shimizu, T. Ogawa, and A. Sakaki, *Phys. Rev. B* **45**, 11338 (1992).
- [10] R. Loudon, *Am. J. Phys.* **27**, 649 (1959).
- [11] T. Ogawa and T. Takagahara, *Phys. Rev. B* **44**, 8138 (1991).
- [12] Y. Nagamune, Y. Arakawa, S. Tsukamoto, and M. Nishioka, *Phys. Rev. Lett.* **69**, 2963 (1992).
- [13] U. Rössler, *Solid State Commun.* **65**, 1279 (1988).
- [14] We should point out that both electrons and excitons in a harmonic potential (somewhat similar to our case) should exhibit a parabolic energy shift vs magnetic field at low fields. However, electrons recover the usual Landau shift (linear in the field) when the cyclotron diameter equals the wire width $2[\hbar/(eR)]^{1/2}(2n+1)^{1/2} \geq L_x$, where $n = 0, 1, \dots$ is the Landau quantum number. In our wires, any free-carrier shift would display a change from parabolic to linear (with Landau level slope) between 4 and 5 T. On the contrary, the observed shift is the typical diamagnetic exciton shift.
- [15] We have used the following parameters: for the height of the confinement potential $V_e^c = 0.15$ eV, $V_h^c = 0.05$ eV and for the effective masses $m_e^* = 0.067m_e$, $m_h^* = 0.34m_e$.